APL Photonics

RESEARCH ARTICLE | JUNE 04 2025

High-throughput wide-field multispectral FLIM system based on a 16-channel silicon photomultiplier array

Elisabetta Avanzi ; Valerio Gandolfi ; Andrea Costa ; Alberto Ghezzi ; Nicola Lusardi ; Fabio Garzetti ; Enrico Ronconi ; Gabriele Bonanno ; Angelo Geraci ; Cosimo D'Andrea ; Andrea Farina ; Alberto Dalla Mora ; Laura Di Sieno

APL Photonics 10, 066104 (2025)
https://doi.org/10.1063/5.0254427

High-throughput wide-field multispectral FLIM system based on a 16-channel silicon photomultiplier array

Cite as: APL Photon. 10, 066104 (2025); doi: 10.1063/5.0254427
Submitted: 22 December 2024 • Accepted: 8 May 2025 •
Published Online: 4 June 2025

Elisabetta Avanzi,[1] Valerio Gandolfi,[1] Andrea Costa,[2] Alberto Ghezzi,[1] Nicola Lusardi,[2] Fabio Garzetti,[2] Enrico Ronconi,[2] Gabriele Bonanno,[2] Angelo Geraci,[2] Cosimo D'Andrea,[1,3,4] Andrea Farina,[4,a)] Alberto Dalla Mora,[1] and Laura Di Sieno[1]

AFFILIATIONS

[1] Dipartimento di Fisica, Politecnico di Milano, Piazza L. da Vinci 32, 20133 Milano, Italy
[2] Dipartimento di Elettronica, Informazione e Bioingegneria, Politecnico di Milano, Piazza L. da Vinci 32, 20133 Milano, Italy
[3] Center for Nano Science and Technology, Istituto Italiano di Tecnologia, Via Raffaele Rubattino, 81, 20134 Milano, Italy
[4] Istituto di Fotonica e Nanotecnologie, Consiglio Nazionale delle Ricerche, Piazza L. da Vinci 32, 20133 Milano, Italy

[a)] **Author to whom correspondence should be addressed:** andrea.farina@cnr.it

ABSTRACT

Fluorescence microscopy is nowadays one of the most diffused techniques to study photophysical processes and molecular interactions in both biomedical and material science fields. Since each fluorophore is characterized by a specific emission spectrum and lifetime, it is essential not only to spatially localize its position but also to measure its spectral and temporal properties with a multispectral fluorescence lifetime imaging microscope (λFLIM). Moreover, to study rapidly evolving samples, a measurement system capable of fast acquisitions is needed. λFLIM systems are currently limited on acquisition speed and cannot reach high throughput. In this work, we propose a novel wide-field multispectral fluorescence lifetime imaging microscope based on a 16-channel silicon photomultiplier (SiPM) array. Our system, thanks to the SiPM technology along with the single pixel camera and compress sensing approaches is able to acquire multidimensional measurements (space, spectrum, and time) at high frame rate. We validate the system on moving fluorescent samples capturing snapshots at a frame rate of up to 13 fps. The developed system could enable enhanced specificity in real-time fluorescence imaging in biological and biosensing applications.

I. INTRODUCTION

Fluorescence microscopy is a powerful technique for studying photophysical processes across a wide range of applications, from biomedical to material science. Beyond its ability to localize the presence of fluorophores (spatial resolution), it can be exploited to also characterize other fluorescence properties. The emission spectrum, for instance, acts as a unique fingerprint for each fluorophore (spectral resolution), enabling precise differentiation among fluorophores and providing detailed analysis of their spectroscopic properties.[1] Moreover, fluorescence lifetime (temporal resolution) provides a robust tool for studying interactions between the fluorophores and their local microenvironment. The analysis of fluorescence lifetime and its variations offers critical insights into parameters such as pH levels, ion concentrations, and molecular interactions affecting the fluorophore.[2] The most widespread fluorescence imaging systems can offer, in addition to spatial resolution, either spectral (multispectral imaging) or temporal (fluorescence lifetime imaging—FLIM) resolution. However, a multispectral fluorescence lifetime imaging (λFLIM) system, enabling the acquisition of multidimensional datasets at once (spatial, spectral, and temporal information), proves to be a powerful tool to provide a better understanding of complex systems and processes.[3–6]

λFLIM is particularly valuable for studying cellular systems, including investigations into metabolic processes,[7,8] energy transfer mechanisms, and fluorescence resonance energy transfer (FRET).[9,10]

At the same time, it is essential to remember that biological systems are highly dynamic and rapidly evolving (e.g., movement, physiological fluctuations, etc.); therefore, measurements must be conducted at high speed to capture the temporal evolution of these biological processes.

In a typical λFLIM system, the sample is spatially scanned with a pulsed laser beam (pulse width of tens of picoseconds) operating at a high repetition rate (tens of MHz). The fluorescence signal emitted by the sample is dispersed using a spectrometer and collected by a linear array of detectors, whose outputs are sent to one or more time-correlated single-photon counting (TCSPC) modules for acquiring temporal profiles for each spectral channel. By fitting these curves with a multi-exponential model, it is possible to extract the fluorescence lifetimes corresponding to the various spectral channels and spatial points.[3] Other systems substitute the spectrometer with a set of bandpass filters to filter fluorescence in different spectral bands and send light to different detectors, thus decreasing the complexity of the setup although strongly reducing the multispectral capability.[4,5] In any case, the main criticality of these systems lies in the raster scan procedure, which makes the acquisition inefficient and slow because only one point of the sample is illuminated at time and the image is formed only once the scanning is completed. This limits the maximum frame rate achievable, particularly when the fluorescence signal from the sample is low.

In this context, recent years have seen significant interest in the development of high-throughput λFLIM systems to minimize measurement times while preserving a multidimensional dataset.[11] These advancements aim to achieve an optimal balance between acquisition speed and the informational richness provided by multidimensional data collection. This goal can be achieved through improvements in hardware systems (e.g., electronic and optical components) combined with new measurement schemes. In particular, the single-pixel camera (SPC) is a novel detection scheme based on structured wide-field illumination and a single-pixel detector. Its basic idea is to measure the inner products between the image and many structured illumination patterns, and then, through an inversion process, it is possible to reconstruct the image.[12] Furthermore, SPC can be well combined with compressive sensing (CS) techniques,[13,14] which enable illumination with a number of patterns (M) smaller than the total number of pixels (N), potentially reducing the number of patterns to as little as 10% of the total pixels. This approach combines the advantages of wide-field acquisition with the enhanced performances (e.g., temporal and spectral) of a single-pixel detector while reducing measurement time thanks to compressive sensing. A λFLIM system based on SPC has been already proposed, demonstrating the possibility to minimize acquisition times to a few seconds per frame.[6] However, its speed is constrained by the detection chain, which, being based on a photomultiplier tube (PMT) detector and a single TCSPC board, limits the maximum photon count rate over all spectral channels.

A recent study has overcome this limitation by using a SiPM detector. Thanks to the SiPM technology, which offers high single-photon temporal resolution (tens of picoseconds), excellent detection efficiency (up to 30% at 600 nm), high-throughput (tens of millions of counts per second), and a large active area (a few mm^2), they have been able to acquire wide-field SPC FLIM at video rates of up to 20 fps.[15] Nevertheless, the multispectral capability has been completely lost in that system because all signals were directed to a single-channel SiPM detector.

However, the possibility of scaling a single SiPM into an array of SiPMs coupled with a spectrometer could pave the way for multidimensional data collection, providing deeper insights into the sample's spectral behavior in addition to the existing lifetime and spatial information.

In this work, we propose a novel high-throughput wide-field multispectral TCSPC-FLIM system based on a CS-SPC scheme, incorporating a spectrometer equipped with an array of 16 independent SiPMs. The system is characterized and validated with both static and video-rate measurements of fluorescent samples applying different analysis methods of the multidimensional dataset. In particular, we show the applicability of our system to fast λFLIM measurements, enabling multispectral time-resolved imaging of the sample's dynamic evolution at frame rates of up to 13 fps. Moreover, it is worth noting that, leveraging commercially available components, our system is cost-effective while achieving a high level of performance and versatility.

II. MATERIALS AND METHODS

A. Description of the optical setup

A scheme of the setup is shown in Fig. 1. Fluorescence light excitation is provided by a mode-locked supercontinuum laser (SC-450, Fianium Inc.) with a repetition rate of 40 MHz and pulse duration of few tens of ps. A 10 nm bandpass filter (F1) selects the desired excitation wavelength. The laser beam, expanded and collimated by lens L1, is sent on a digital micromirror device (DMD) (V-7000, ViaLUX GmbH), which acts as a reflective spatial light modulator (SLM) to create structured illumination patterns needed for CS-SPC acquisitions. The light from the DMD is collected by lens L2 (f = 200 mm, AC508-200-A, Thorlabs Inc.) and reflected by a dichroic mirror (DM) toward a 40× microscope objective (Plan N 40×, NA 0.65, infinity corrected, Olympus Corp.) that focuses the illumination pattern onto the sample slide in a 150 × 150 μm^2 field of view. Then, emitted fluorescence light, collected by the same objective, is filtered by a long pass filter (F2) to remove residual scattered excitation light. According to the excitation wavelength, we use a proper configuration for DM and F2. A 50:50 beam splitter (BS) (BSW10R, Thorlabs Inc.) separates light into two different detection paths. In the first one, a lens (L3, f = 200 mm, AC254-200-A, Thorlabs Inc.) and a CMOS camera (C13440-20CU, Hamamatsu) allow acquiring a high-resolution intensity image of the sample. On the other detection path, light is sent to a spectrometer (Kymera 193i, Andor) by means of a 550 μm optical fiber. A 1200 grooves/mm diffraction grating disperses input light over the 16-channel SiPM array detector, further described in Sec. II B, which allows measuring the multispectral time-resolved signal of the SPC acquisition. Each channel of the detector collects a bandwidth with full width at half maximum (FWHM) of about 7 nm, which represents the spectral resolution of our system. We point out that, thanks to the use of a commercial spectrometer, we can easily change the diffraction grating and adapt the spectral resolution and the spectral range to the experiment. A spectral calibration was performed to assign an appropriate central wavelength to each channel of the array. Moreover, the differences in collection efficiency of each channel have been compensated using a reference spectrum collected by using a

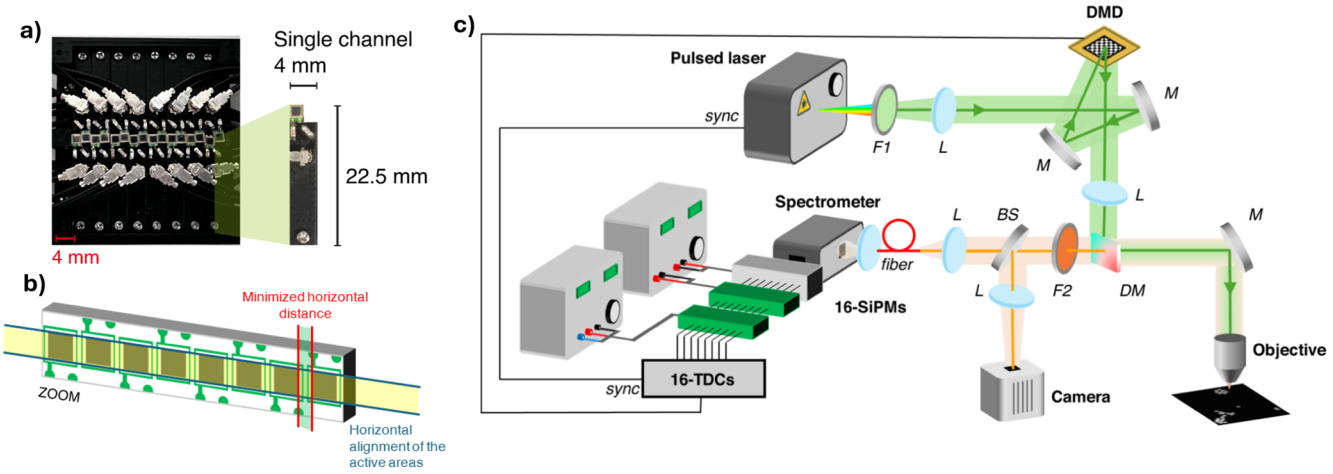

FIG. 1. (a) Image of the 16-channel array, with a zoomed-in view of a single channel and its dimensions. (b) Detail about the alignment of each SiPM for spectroscopy. (c) The experimental setup. F: filter, L: lens, M: mirror, DMD: Digital Micromirror Device, DM: dichroic mirror, BS: beam splitter.

commercial spectrometer (USB2000, Ocean Optics). The detector is finally connected to a timing system, further described in Sec. II B, which is hardware synchronized with the laser and the DMD, and allows collecting in parallel the time-resolved fluorescence signal for each channel of the SiPM array. The temporal instrument response function (IRF) has been measured removing F1 and F2 and substituting DM and the sample with a beam splitter and a reflective microscope slide, respectively, thus shining white light into the detection chain. The average FWHM of the IRF over the 16 channels is 150 ps.

B. Description of the detection chain

The 16-channel SiPM array is composed of 16 independent printed circuit boards (PCBs), each equipped with a front-end circuit designed to include both biasing and read-out functionalities, to preserve the signal integrity and to limit the crosstalk among channels. The design of the PCB aims to minimize the size of each single channel (its dimensions are 4×22.5 mm^2). The 16 SiPMs are then mounted on a custom 3D printed holder, as shown in Fig. 1(a). In particular, the selected geometry is optimized for spectroscopic purposes to collect light dispersed in one direction. Indeed, particular attention has been dedicated to minimize the spacing between channels, while keeping all of them on the same horizontal line, as shown in Fig. 1(b). Each detection channel contains a 1.3×1.3 mm^2 active area SiPM (S13360-1350PE, Hamamatsu). Each SiPM operates at an excess voltage of 6 V (breakdown voltage V_{bd} = 51.3 V), has a dark-count rate (DCR) of about 144 kcps (counts per second), and has a minimum single-photon timing resolution (SPTR) of 65 ps. To meet the signal characteristics that the timing electronics can accept (voltage amplitude between 0 and 3.3 V), the array is coupled with an amplification stage (block A of Fig. 1). Moreover, to feed the time-to-digital converters (TDCs) the signal with the correct polarity, a low voltage TTL comparator stage composed of 16 independent PCBs has been inserted (block B of Fig. 1).

The timing system consists of a high-performance 17-channel (16 for inputs and 1 dedicated to a reference synchronism signal, e.g., a pulsed laser) tapped delay-line time-to-digital converter (TDL-TDC) interfaced with 16 histogramming modules,[16] all implemented in a Xilinx 28 nm 7-Series Kintex-7 325T Field-Programmable Gate Array (FPGA) on a custom PCB designed to maximize signal integrity and minimize crosstalk between channels. Each channel is equipped with a low-jitter threshold comparator (ADCMP607, Analog Devices Inc.) and read out using the Multi-COBS protocol over a high-speed USB 3.0 interface. In particular, each of the 17 channels of the TDL-TDC is capable of detecting timestamps with a resolution of 12 ps rms and a dead time of 12 ns.[17] The measured timestamps are transmitted to the 16 histogramming modules, each of which can calculate in real time, at up to 250 Msamples/s, the distribution of time delays over 4096 tunable-width bins for each of the 16 channels, using the synchronism channel as a reference. This distribution, according to the TCSPC technique, reflects the time-resolved optical signal at the detector. In addition, each histogram includes an innovative fast time trigger (FTT), which allows sending contiguous histogram windows at high rate, accumulating coincidences for as short as 150 μs upon the occurrence of specific external trigger events on one acquisition channel (i.e., the DMD signal) or from a user-programmable internal timer. A suitable FTT functionality has been developed since the application in this work requires synchronization between the measurement device and the movement of the setup (e.g., DMD, in our setup). The 16-channel timing system module has remarkable compactness (about $22 \times 11 \times 6$ cm^3) and low power consumption (<10 W) with respect to similar systems, allowing a potential minimization of the size of the detection chain.

C. Samples and data analysis

The proposed system has been validated by measuring two types of fluorescent samples. First, a mix of two different kinds of fluorescent beads, diluted in water and deposited on a glass slide,

was measured to validate the capabilities of the system in retrieving image, spectrum, and time. The first kind of bead has a diameter of 15 μm with absorption peak at 530 nm and emission peak at 580 nm (Cat. No. 2228, Phosphorex), while the second one has a diameter of 10 μm with absorption peak at 465 nm and emission peak at 480 nm (FH-10052-2, Spherotech). The second sample is composed of bovine pulmonary artery endothelial (BPAE) cells fixed on a glass slide (FluoCells#1 F36924, Invitrogen), stained with MitoTracker Red CMXRos (exc: 579 nm/em: 599 nm) to label mitochondria and Alexa Fluor 488 (exc: 505 nm/em: 512 nm) to label F-actin.

Single-pixel camera measurements were acquired by projecting with the DMD a set of patterns generated by reshaping into a $n \times n$ squared matrix the first M rows of a scrambled Hadamard matrix ($H_{n\times n}$), built by randomly permuting rows and columns of a Hadamard matrix order n. For video-rate acquisitions, the same sequence of patterns was repeated so as to acquire multiple frames. The -1 entries in $H_{n\times n}$ were substituted with 0 in order to have patterns compatible with the DMD. In this way, as demonstrated in a previous study,[18] we avoid the differential measurement typically needed when using Hadamard patterns, which would require projecting $2M$ pattern, thus reducing acquisition times without compromising imaging quality. We used a Hadamard matrix of order $n = 32$ (then a number $N = n \times n = 1024$ of patterns, leading to an image with the same number of pixels in total), and we projected only $M = 256$ patterns, corresponding to a compression ratio (defined as $CR = 1 - M/N$) of 75%. This choice of n and M comes from a trade-off between spatial resolution, image quality, and acquisition speed with the aim to minimize the latter one while keeping the first two acceptable. Indeed, an increase in image resolution would require a much higher number of patterns, compromising the possibility to reach high frame rate acquisition, needed to follow the sample dynamics.

The SPC image reconstruction requires to solve an inverse problem where the reconstructed image, unrolled in a vector $x_{N\times 1}$, is computed from the measurements $m_{M\times 1}$ by a matrix inversion $x_{N\times 1} = W^{-1}_{M\times N} m_{M\times 1}$, where $W_{M\times N}$ is the measurement matrix containing each pattern reshaped in a row. Since we did not project the complete set of Hadamard patterns ($M < N$), the problem is underdetermined and needs some regularization terms to be solved. We exploited the total variation minimization by augmented Lagrangian and alternating direction algorithms (TVAL3), which allows solving the underdetermined problem $x_{N\times 1} = W^{-1}_{M\times N} m_{M\times 1}$ by minimizing the gradient variation over the image $x_{N\times 1}$.[19] Since for each pattern the 16-channel SiPM array captures both time decay and spectrum of the fluorescence emission of the sample, by applying the SPC reconstruction to each time bin and spectral channel, we can finally get a multidimensional dataset in which each pixel of the image embeds both spectral and temporal information.

To retrieve the lifetime values, we interpolated the time-resolved curves, exploiting the MATLAB fit function based on the non-linear least square method, with a biexponential model $f(t) = A_1 \exp(-t/\tau_1) + A_2 \exp(-t/\tau_2) + c$, and we calculated the average lifetime $\tau_{avg} = (A_1\tau_1 + A_2\tau_2)/(A_1 + A_2)$ of the fluorophore. The fitting procedure was applied to each pixel of the SPC reconstructed image for each spectral channel.

Since the SPC reconstruction and fitting procedure of the entire dataset (4096 time bins of 9 ps each × 16 spectral channels) would require about 620 s per frame, considering the high number of frames measured during the video-rate acquisition, we decided to re-bin raw data in temporal channels of 50 ps width and two spectral bands SB1 and SB2, thus reducing the reconstruction time to about 60 s per frame (the computation times refer to a laptop with 2.30 GHz Intel Core i7-10510U CPU and 16 GB RAM). However, the raw dataset was still used to retrieve the spectrum for each acquired frame.

To further speed-up the measurement reconstruction, keeping all the advantages of the multidimensionality of the dataset, we explored global approaches of reconstruction such as the fast fit method previously proposed by the authors,[20] which allows us to strongly reduce the computational times. This method consists in a global fit of a 2D time-spectrum map to retrieve the values of lifetimes τ_i (i is the number of independent temporal components in the sample) and their decay associated spectrum (DAS_i).[21] In our case, the 2D time-spectrum map was obtained by summing raw data of all projected patterns in the analyzed frame. This is followed by a linear fit to find the contribution of each τ_i (and DAS_i) to each measured pattern. In the end, after image reconstruction with TVAL3 algorithm as mentioned above, we obtain an image showing the spatial distribution of the ith component associated with τ_i (and DAS_i) found with global analysis. With this method, about 3 s per frame are needed to reconstruct the measurement. In particular, less than 3 s are needed for the global analysis part and about 100 ms to retrieve the FLIM images. It is worth noting that global analysis can be done once for all the frames, thus further decreasing computational times. The short computational times then make the fast fit method an interesting algorithm to reconstruct the multiple fames of the video-rate measurements.

III. RESULTS AND DISCUSSION

A. Fluorescent beads

First, measurements were performed on fluorescent beads. The excitation wavelength was 480 nm to excite both kinds of beads. The dichroic mirror and long pass filter to cut excitation light had a cut-on wavelength of 505 and 500 nm, respectively. The laser power on the sample was set to 16 μW, corresponding to a maximum photon rate of 1.8 Mcps/ch at the detector. The sample was illuminated with 256 patterns with a total acquisition time of 76.8 ms (exposure time for each pattern is 300 μs). The measurements were repeated one after the other 150 times (total acquisition time of 11.5 s), while the sample was manually moved under the objective by means of a translation stage. All the acquisitions have been merged into a movie, which, with the exposure time set, has a frame rate of 13 frames per second (fps). Thanks to the beam splitter (BS in Fig. 1), both a SPC measurement and a high-resolution image with the CMOS camera (exposure time of 76.8 ms) are acquired simultaneously. The analysis workflow described in the first paragraph of Sec. II C was applied to each frame of the movie. Given the fluorescence emission spectrum measured for the beads (see Fig. S1 in the supplementary material), the two selected spectral bands were: SB1 (512–532) nm and SB2 (580–600) nm. In Fig. 2 (Multimedia available online), a single frame of the movie is shown.

To quantify similarity between the SPC reconstructed image [Fig. 2(b)] and the CMOS reference image [Fig. 2(a)], we computed the peak signal to noise ratio (PSNR) and the structure similarity index (SSIM) of the SPC image obtained integrating over time and

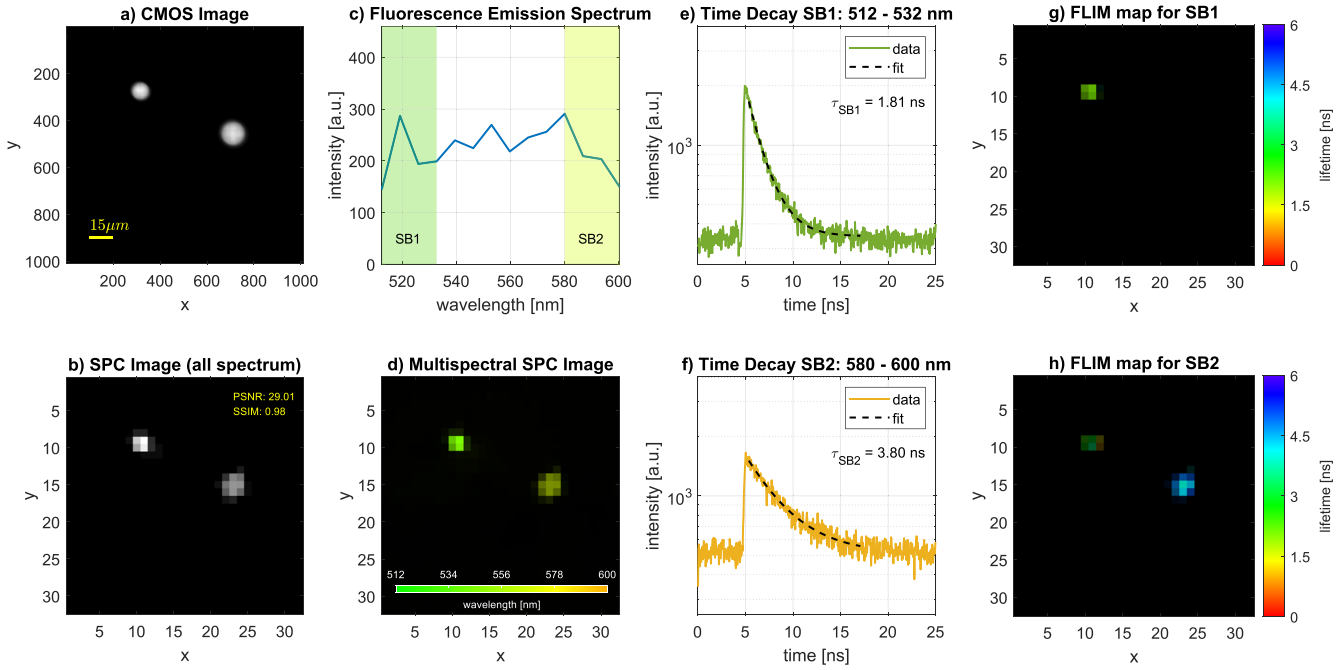

FIG. 2. One frame of the movie of fluorescent beads. (a) High-resolution reference CMOS image; (b) SPC image obtained integrating over all time and spectral channels; (c) spectrum of the observed field of view; (d) multispectral SPC image colored according to the spectrum in each pixel; (e) time decay of the fluorophore emitting in SB1, obtained integrating over the whole field of view; (f) time decay of the fluorophore emitting in SB2, obtained integrating over the whole field of view; (g) map of average lifetime for spectral band SB1; and (h) map of average lifetime for spectral band SB2. (Multimedia Available online)."http://10.1063/5.0254427.1"

spectrum, with respect to the CMOS image. In this way, the two metrics include both the effect of lower resolution of SPC and the possible degradation from the reconstruction process. The two effects have been separated in Fig. S4, where we show the comparison between the high-resolution CMOS image, and its downsampling to match the SPC resolution and the SPC image, with the PSNR and SSIM values along frames. The average value of PSNR over all the frames of the movie is 26.8 (minimum: 23.0, maximum: 31.6), while for SSIM, we have 0.96 (minimum: 0.93, maximum: 0.99). These values confirm a good similarity between the SPC reconstructed image and the CMOS reference image.

Concerning the spectrum, we see that in Fig. 2(d), which shows the multispectral image colored according to the spectrum associated with each pixel, the two different beads correctly assume different colors according to their different emission spectrum. In the movie, it is possible to see how the spectrum in panel (c) changes shape according to the kind of beads in the field of view. Indeed, in the first frames, we have only 10 μm beads, and in the spectrum, we see only the tail of the emission peak at 480 nm. At $t = 5$ s, the field of view shows only a 15 μm bead, and now the spectrum, as expected, exhibits a peak at 580 nm while the tail of the 480 nm peak has disappeared. Then, in the next frames, as in Fig. 2(c), the field of view contains both kinds of beads, and the spectrum is the sum of the ones previously observed.

A similar behavior can be seen in panels (d) and (e) of Fig. 2, which show the time-resolved fluorescence decay obtained by integrating the SPC image over all the pixels for the two selected spectral bands. Indeed, the fluorescence signal raises or reduces according to the type of beads present in the field of view.

The multidimensionality of the dataset allowed us to also calculate the average lifetime maps for SB1 [Fig. 2(g)] and SB2 [Fig. 2(h)]. Thanks to the average lifetime maps, we can clearly see that a shorter lifetime is associated with 10 μm beads while a longer lifetime is associated with 15 μm bead. In particular, exploiting all the spatial, spectral, and temporal information, we interpolated the time decays of panels (d) and (e) in order to obtain an average lifetime for each spectral band (i.e., kind of bead). For instance, in the frame shown in Fig. 2, we obtained an average lifetime value of $\tau_{SB1} = 1.81$ ns for SB1 and $\tau_{SB2} = 3.80$ ns for SB2. Averaging over all the frames of the movie, we found $\bar{\tau}_{SB1} = 1.82$ ns and $\bar{\tau}_{SB2} = 3.76$ ns with a standard deviation of less than 10%, showing a good stability over all the acquisitions. Figure S6 shows the average lifetimes for each frame.

Finally, in order to further test the reliability of the measurements, the same sample has been measured, without motion and with a long acquisition time, to enhance the signal to noise ratio. We obtained average lifetime values of $\tau_{SB1} = 1.78$ ns and $\tau_{SB2} = 3.58$ ns, thus a maximum deviation of less than 10% with respect to the ones of the video rate acquisition (see Fig. S1 in the supplementary material). The same dataset was analyzed with the fast fit method described in Sec. II C. Figure 3 (Multimedia available online) shows the results obtained with the fast fit method for the same frame of the movie of Fig. 2.

The lifetimes found by global analysis for the frame shown in Fig. 3 are $\tau_1 = 1.64$ ns and $\tau_2 = 3.64$ ns. The average of lifetimes

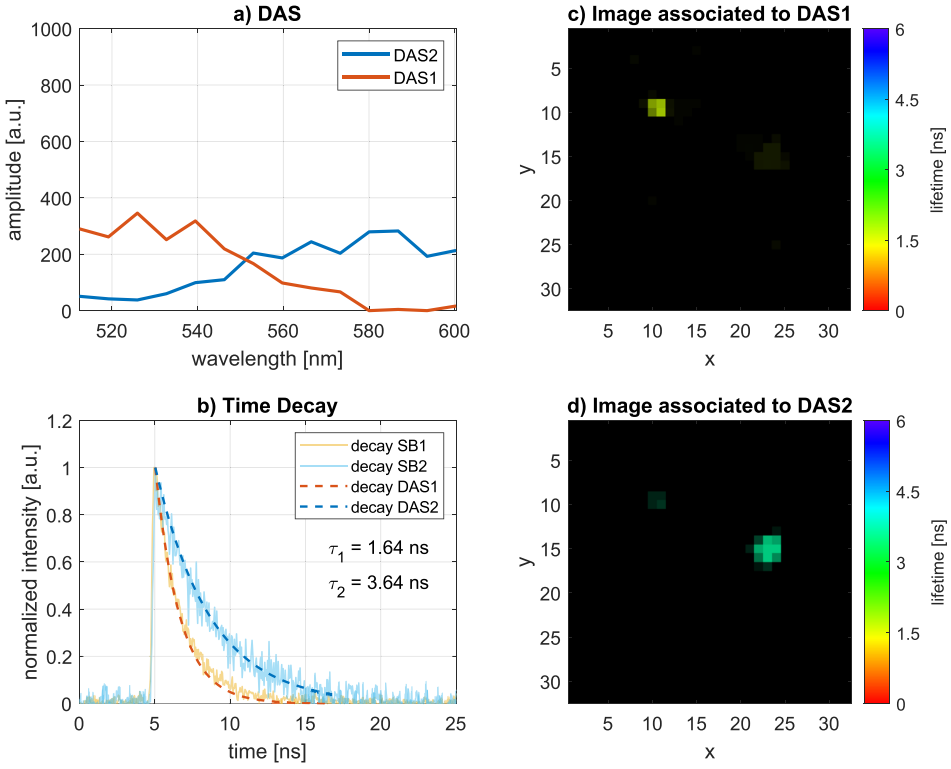

FIG. 3. Fast fit method applied to the fluorescent beads dataset. The figure shows the same frame of the movie reported in Fig. 2. (a) *DAS* for each independent fluorescence component; (b) lifetimes and decays found by global analysis, overlapped with the time decays in previously defined SB1 and SB2; (c) FLIM map associated with first component (τ_1, DAS_1); and (d) FLIM map associated with the second component (τ_2, DAS_2). (Multimedia available online).http//doi.org/10.1063/5.0254427.2

values over all the frames are $\bar{\tau}_1$ = 1.69 ns and $\bar{\tau}_2$ = 3.97 ns, with a standard deviation of less than 10% in both cases (see Fig. S7). These data are in agreement with the lifetimes previously found and their deviation is compatible with the different analysis method. Indeed, as global fit considers the 2D time-spectrum map, it is possible that the lifetimes obtained are not exactly the same obtained by integrating the spectrum over spectral bands and performing a multi-exponential fit.

Looking at the *DAS*s instead and comparing them with the spectrum in Fig. 2 and its correspondent movie, it is possible to note that the spectral fingerprint of the two beads is correctly reproduced over all the movies.

Finally, the two images in Figs. 3(c) and 3(d) show that the longest lifetime is associated with the biggest bead while the shortest lifetime is associated with the smallest beads, as we have already seen in the previous analysis. These results are also in agreement with those obtained applying the fast fit method to the static measurements (see Fig. S2 in the supplementary material).

This confirms that fast fit is a good method for accelerating the reconstruction of our dataset without compromising its multidimensionality.

B. BPAE cells

For the measurements on the BPAE cells, the excitation wavelength was set to 520 nm. Consequently, we used a dichroic mirror and a long pass filter with cut-on at 550 nm. The laser power on the sample was set to 250 μW, corresponding to a maximum photon rate of 1 Mcps/ch. The sample was illuminated with 256 patterns for a total acquisition time of 500 ms (single pattern exposure time was 2 ms). We acquired 50 measurements, one after the other, with the parallel acquisition of SPC and CMOS images, while the sample was manually moved by means of a translation stage. All acquisitions have been finally merged into a movie that in this case has a frame rate of 2 fps and a duration of 25 s. Figure 4 (Multimedia available online) shows a single frame of the obtained movie.

After selecting two spectral bands [SB1 (570–590) nm and SB2 (600–630) nm], we reconstructed the two corresponding images that we show in different colors and overlapped to the CMOS image in Fig. 4(b). Then, as for the previous sample, we retrieved the fluorescence time decays for the whole field of view [Figs. 4(c) and 4(d)] and the average lifetime maps [Figs. 4(e) and 4(f)] for the two spectral bands. In this way, with SB1 we are able to observe the tail of the emission peak at 512 nm of Alexa Fluor 488 used to mark the F-actin and with SB2, the emission peak at 599 nm of MitoTraker Red CMXRos used to mark the mitochondria. In fact, comparing the two SPC images for SB1 [Fig. 4(b) yellow] and SB2 [Fig. 4(b) red] and the high-resolution CMOS image, we note that the image corresponding to SB1 is spread over all the cell and it has higher intensity at the cellular membrane where F-actin is more concentrated, while the image corresponding to SB2 is restricted to the central part of the cell where mitochondria are present. The PSNR and SSIM were computed between the SPC and CMOS images, as discussed for the beads sample. We obtained an average PSNR value, over all the frames of the movie, of 13.0 (minimum: 11.0, maximum: 16.1) and an average

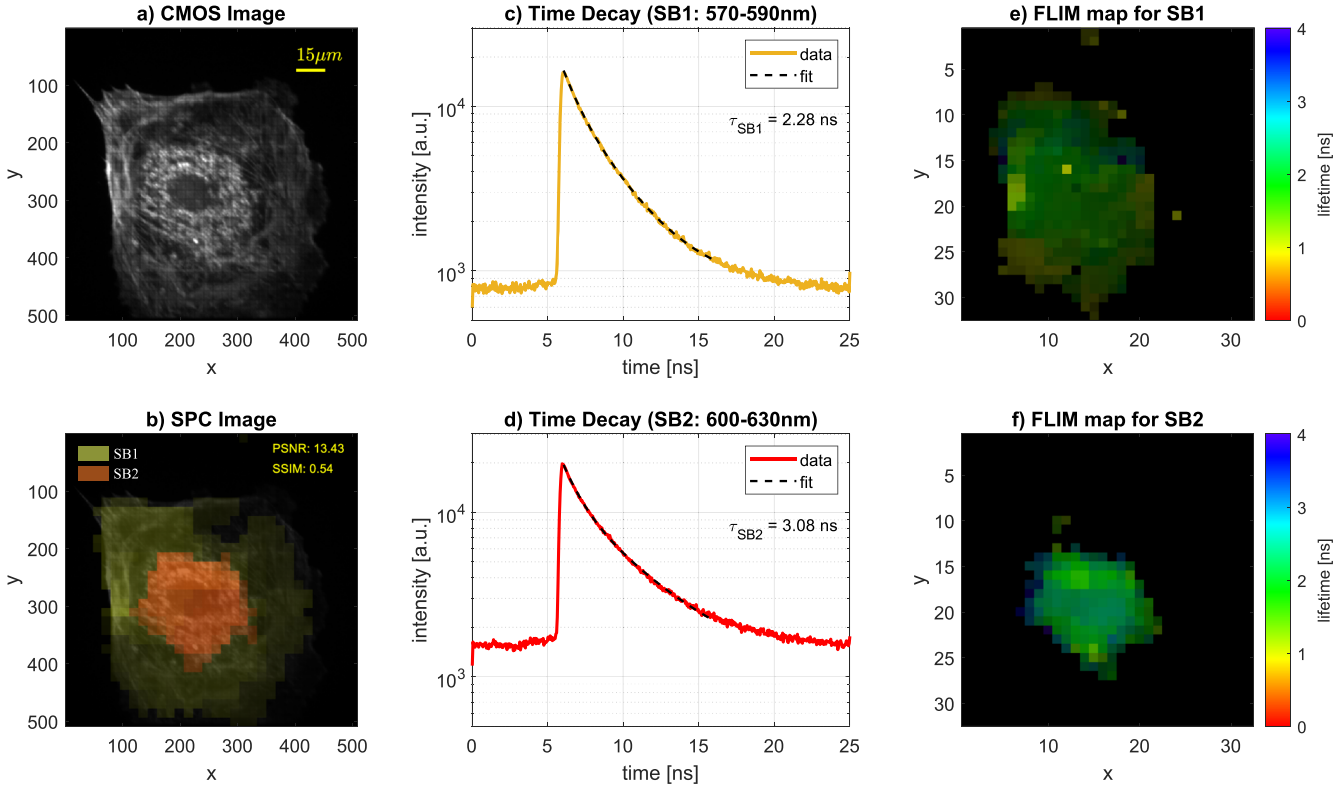

FIG. 4. One frame of the movie of BPAE cells. (a) High-resolution reference CMOS image; (b) SPC images obtained in two different spectral bands (SB1 in yellow and SB2 in red) overlapped to the CMOS image; (c) time-resolved fluorescence decay in SB1, corresponding to the yellow region in panel (b); (d) Time-resolved fluorescence decay in SB2, corresponding to the red region in panel (b); (e) map of the average lifetime for SB1; and (f) map of the average lifetime for SB2. (Multimedia available online).http//doi.org/10.1063/5.0254427.3

SSIM value of 0.59 (minimum: 0.48, maximum: 0.69). These values are notably low: indeed, due to both the low resolution of the SPC and the high compression ratio of the measurement, the small details of the cells, such as single mitochondria and actin filaments, are not sharp. However, the overall shape of the cell is correctly reproduced in the SPC image, allowing for its localization in space and mapping of spectral and temporal properties of fluorescence (for more details, see Fig. S5).

Finally, fitting the time decays in SB1 and SB2, we obtained mean values of the average lifetimes over all the movies, of $\bar{\tau}_{SB1}$ = 2.26 ns and $\bar{\tau}_{SB2}$ = 3.11 ns, respectively, with variation of less than 5% (the values for each frame are shown in Fig. S8). In addition, for this sample, as a further comparison, we made a reference static measurement. We obtained average lifetime values of τ_{SB1} = 2.34 ns and τ_{SB2} = 2.84 ns (see Fig. S3). The variability of the estimated lifetimes is less than 10%, thus confirming a good agreement between the measurements.

The measurements presented above demonstrate the capability of our system to collect multispectral fluorescence lifetime snapshots that, thanks to the linear array of 16 SiPMs and the reading electronics, can reach acquisition frequencies greater than 10 fps. This could enable real-time fluorescence imaging in biological and biosensing applications with both lifetime and emission spectrum information.

IV. CONCLUSION

In this work, we have proposed, designed, and characterized a novel high-throughput wide-field multispectral fluorescence lifetime microscopy system based on a 16-channel silicon photomultiplier array. In particular, the use of a novel SiPM array coupled with a microscope based on compressive sensing and a single pixel camera allows preserving the high information content multidimensional dataset (space, spectrum, and time), while strongly increasing the throughput up to 13 fps. The system has been validated with both static and video rate measurements of fluorescent samples applying different analysis methods to the multidimensional dataset. Indeed, the very high dimensionality of the dataset requires some strategies to reconstruct the measurements in a short time. In particular, a fast fitting method, which allows us to provide in few hundreds of ms the spectral images associated with the fluorescence, was exploited to speed up measurements reconstruction. Future work will be devoted to further decreasing the reconstruction time by exploiting faster algorithms and their parallelization over graphics processing units (GPUs) to enable real-time imaging.[22] Moreover, to improve the low spatial resolution of the SPC acquisition, the implementation of data fusion algorithms with the CMOS image will be exploited to enhance the spatial resolution while preserving spectral

and temporal information.[6,23] In this frame, machine learning is a novel and promising tool that could be explored to improve both SPC acquisition and reconstruction by enhancing spatial resolution while reducing measurement speed and postprocessing computational times.[24–26] Finally, we want to highlight that our system could be extended and adapted to other applications. For instance, the parallel detection of spectrum and time is often needed in the field of diffuse optics for fast measurements of optical properties[27–29] or optical tomography.[30] Otherwise, the capability to map spatial distribution of light with spectral and temporal resolution could also be employed in the field of optical computing, where it has been applied for years with different techniques,[31,32] or multispectral LiDAR systems.[33] Thus, our advancements are not only limited to fluorescence microscopy, for which we enabled the possibility to capture fast biological processes with spectral and lifetime information, but also can give benefit to any other applications where multidimensionality (space, spectrum, and time) and high-throughput are required.

SUPPLEMENTARY MATERIAL

The supplementary material provides additional figures and additional measurements on the same samples presented in Sec. II C done with our wide-field multispectral TCSPC-FLIM system based on a 16-channels SiPM array.

ACKNOWLEDGMENTS

The authors acknowledge financial support from the European Union's NextGenerationEU Programme with the I-PHOQS Infrastructure (Grant Nos. IR0000016, ID D2B8D520, and CUP B53C22001750006) "Integrated infrastructure initiative in Photonic and Quantum Sciences," the Ministero dell'Università e della Ricerca with PRIN2020 (Grant No. 2020WMSNBL) and PRIN 2022 (Proactive, 2022NEJZ2C), and CONcISE-DN under the Marie Sklodowska-Curie program (GA No. 101072354). The authors thank TEDIEL S.r.l. for providing the timing electronics prototype for the experiment. Views and opinions expressed are however those of the author(s) only and do not necessarily reflect those of the European Union or the European Research Executive Agency. Neither the European Union nor the granting authority can be held responsible for them.

AUTHOR DECLARATIONS

Conflict of Interest

The authors have no conflicts to disclose.

Author Contributions

Elisabetta Avanzi and Valerio Gandolfi contributed equally to this paper.

Elisabetta Avanzi: Data curation (equal); Investigation (equal); Writing – original draft (equal). **Valerio Gandolfi**: Data curation (equal); Formal analysis (lead); Investigation (equal); Software (equal); Visualization (lead); Writing – original draft (equal). **Andrea Costa**: Data curation (equal); Writing – original draft (equal). **Alberto Ghezzi**: Software (lead); Writing – review & editing (equal). **Nicola Lusardi**: Investigation (equal); Writing – review & editing (equal). **Fabio Garzetti**: Investigation (equal); Writing – review & editing (equal). **Enrico Ronconi**: Investigation (equal); Writing – review & editing (equal). **Gabriele Bonanno**: Data curation (equal); Writing – review & editing (equal). **Angelo Geraci**: Funding acquisition (equal); Writing – review & editing (equal). **Cosimo D'Andrea**: Conceptualization (equal); Funding acquisition (equal); Methodology (equal); Writing – original draft (equal). **Andrea Farina**: Conceptualization (equal); Funding acquisition (equal); Methodology (equal); Writing – review & editing (equal). **Alberto Dalla Mora**: Conceptualization (equal); Funding acquisition (equal); Methodology (equal); Writing – review & editing (equal). **Laura Di Sieno**: Conceptualization (equal); Funding acquisition (equal); Methodology (equal); Writing – original draft (equal).

DATA AVAILABILITY

The data that support the findings of this study are available from the corresponding author upon reasonable request.

REFERENCES

[1] L. Gao and R. T. Smith, J. Biophotonics **8**, 441 (2015).
[2] R. Datta, T. M. Heaster, J. T. Sharick, A. A. Gillette, and M. C. Skala, J. Biomed. Opt. **25**, 071203 (2020).
[3] W. Becker, A. Bergmann, and C. Biskup, Microsc. Res. Tech. **70**, 403 (2007).
[4] S. Shrestha, B. E. Applegate, J. Park, X. Xiao, P. Pande, and J. A. Jo, Opt. Lett. **35**, 2558 (2010).
[5] X. Zhou, J. Bec, D. Yankelevich, and L. Marcu, Opt. Express **29**, 20105 (2021).
[6] A. Ghezzi, A. J. M. Lenz, F. Soldevila, E. Tajahuerce, V. Vurro, A. Bassi, G. Valentini, A. Farina, and C. D'Andrea, APL Photonics **8**, 046110 (2023).
[7] A. V. Meleshina, V. V. Dudenkova, M. V. Shirmanova, V. I. Shcheslavskiy, W. Becker, A. S. Bystrova, E. I. Cherkasova, and E. V. Zagaynova, Sci. Rep. **6**, 21853 (2016).
[8] M. Evers, N. Salma, S. Osseiran, M. Casper, R. Birngruber, C. L. Evans, and D. Manstein, Sci. Rep. **8**, 8757 (2018).
[9] A. Margineanu, J. J. Chan, D. J. Kelly, S. C. Warren, D. Flatters, S. Kumar, M. Katan, C. W. Dunsby, and P. M. W. French, Sci. Rep. **6**, 28186 (2016).
[10] H. Wallrabe and A. Periasamy, Curr. Opin. Biotechnol. **16**, 19 (2005), analytical biotechnology.
[11] J. Park and L. Gao, Curr. Opin. Solid State Mater. Sci. **30**, 101147 (2024).
[12] G. M. Gibson, S. D. Johnson, and M. J. Padgett, Opt. Express **28**, 28190 (2020).
[13] M. F. Duarte, M. A. Davenport, D. Takhar, J. N. Laska, T. Sun, K. F. Kelly, and R. G. Baraniuk, IEEE Signal Process. Mag. **25**, 83 (2008).
[14] M. F. Duarte and Y. C. Eldar, IEEE Trans. Signal Process. **59**, 4053 (2011).
[15] A. Ghezzi, E. Avanzi, A. G. Fleitas, L. Di Sieno, A. Dalla Mora, S. Santabarbara, A. Bassi, G. Valentini, A. Farina, and C. D'Andrea, Opt. Express **32**, 24553 (2024).
[16] A. Costa, N. Corna, F. Garzetti, N. Lusardi, E. Ronconi, and A. Geraci, IEEE Access **10**, 47524 (2022).
[17] N. Lusardi, F. Garzetti, G. Bulgarini, R. Gourgues, J. Los, and A. Geraci, in *2016 IEEE Nuclear Science Symposium, Medical Imaging Conference and Room-Temperature Semiconductor Detector Workshop (NSS/MIC/RTSD)* (IEEE, 2016), pp. 1–4.
[18] R. Sun, J. Long, Y. Ding, J. Kuang, and J. Xi, Photonics **10**, 395 (2023).
[19] C. Li, W. Yin, H. Jiang, and Y. Zhang, Comput. Optim. Appl. **56**, 507 (2013).
[20] A. Ghezzi, A. Farina, V. Vurro, A. Bassi, G. Valentini, and C. D'Andrea, Opt. Lett. **49**, 278 (2024).
[21] I. H. M. van Stokkum, D. S. Larsen, and R. van Grondelle, Biochim. Biophys. Acta, Bioenerg. **1657**, 82 (2004).

[22]R. Stojek, A. Pastuszczak, P. Wróbel, M. Cwojdzińska, K. Sobczak, and R. Kotyński, Sensors **24**, 8139 (2024).
[23]F. Soldevila, A. J. M. Lenz, A. Ghezzi, A. Farina, C. D'Andrea, and E. Tajahuerce, Opt. Lett. **46**, 4312 (2021).
[24]C. F. Higham, R. Murray-Smith, M. J. Padgett, and M. P. Edgar, Sci. Rep. **8**, 2369 (2018).
[25]A. L. Mur, P. Leclerc, F. Peyrin, and N. Ducros, Opt. Express **29**, 17097 (2021).
[26]H. Liu, X. Chang, J. Yan, P. Guo, D. Xu, and L. Bian, Opt. Lett. **48**, 4392 (2023).
[27]A. Bassi, J. Swartling, C. D'Andrea, A. Pifferi, A. Torricelli, and R. Cubeddu, Opt. Lett. **29**, 2405 (2004).
[28]F. Lange, L. Giannoni, and I. Tachtsidis, Appl. Sci. **11**, 4616 (2021).
[29]A. Sudakou, F. Lange, H. Isler, P. Lanka, S. Wojtkiewicz, P. Sawosz, D. Ostojic, M. Wolf, A. Pifferi, I. Tachtsidis, A. Liebert, and A. Gerega, Biomed. Opt. Express **12**, 6629 (2021).
[30]D. Lighter, J. Hughes, I. Styles, A. Filer, and H. Dehghani, Biomed. Opt. Express **9**, 1445 (2018).
[31]X. Xu, M. Tan, B. Corcoran, J. Wu, A. Boes, T. G. Nguyen, S. T. Chu, B. E. Little, D. G. Hicks, R. Morandotti *et al.*, Nature **589**, 44 (2021).
[32]M. H. Latifpour, B. J. Park, Y. Yamamoto, and M.-G. Suh, Optica **11**, 932 (2024).
[33]N. Takhtkeshha, G. Mandlburger, F. Remondino, and J. Hyyppä, Sensors **24**, 1669 (2024).